Compartmentalization Directs Assembly of the Signal Recognition Particle†

Tuhin Subhra Maity, Christopher W. Leonard, Marsha A. Rose, Howard M. Fried,‡ and Kevin M. Weeks*

Department of Chemistry, University of North Carolina, Chapel Hill, North Carolina 27599-3290

Received May 4, 2006; Revised Manuscript Received August 29, 2006

ABSTRACT: Many ribonucleoprotein complexes assemble stepwise in distinct cellular compartments, a process that usually involves bidirectional transport of both RNA and proteins between the nucleus and cytoplasm. The biological rationale for such complex transport steps in RNP assembly is obscure. One important example is the eukaryotic signal recognition particle (SRP), a cytoplasmic RNP consisting of one RNA and six proteins. Prior in vivo studies support an "SRP54-late" assembly model in which all SRP proteins, except SRP54, are imported from the cytoplasm to the nucleus to bind SRP RNA. This partially assembled complex is then exported to the cytoplasm where SRP54 binds and forms the SRP holocomplex. Here we show that native SRP assembly requires segregated and ordered binding by its protein components. A native ternary complex forms in vitro when SRP19 binds the SRP RNA prior to binding by SRP54, which approximates the eukaryotic cellular pathway. In contrast, the presence of SRP54 disrupts native assembly of SRP19, such that two RNA-binding loops in SRP19 misfold. These results imply that SRP54 must be sequestered during early SRP assembly steps, as apparently occurs in vivo, for proper assembly of the SRP to occur. Our findings emphasize that spatial compartmentalization provides an additional level of regulation that prevents competition among components and can function to promote native assembly of the eukaryotic SRP.

Intricate ribonucleoprotein (RNP) machines are central to most of the fundamental processes of gene expression including mRNA maturation (mRNPs), translation (the ribosome), and protein trafficking (the signal recognition particle). In eukaryotes, the RNA and protein components of an RNP are synthesized in separate cellular compartments, the nucleus and the cytoplasm, respectively. Thus, in even the simplest RNP assembly pathway, either the protein or the RNA components must be transported through the nuclear envelope. In fact, many RNPs instead assemble via labyrinthine pathways involving both cytoplasmic and nuclear (including nucleolar and Cajal body) phases for which the biological rationale is largely unknown (*1*−*4*).

A currently unexplored possibility is that segregating specific RNP assembly steps into different cellular compartments explicitly facilitates correct and native assembly of some ribonucleoprotein complexes. In this report, we present results of in vitro experiments that provide evidence for just such a mechanism in the biogenesis of the eukaryotic signal recognition particle (SRP), which appears to assemble via a compartmentalized pathway that prevents formation of a misassembled complex.

The eukaryotic SRP is a rod-shaped RNP complex comprised of a single RNA (∼300 nts in mammals and ∼500 nts in yeast) and six proteins (Figure 1A) that functions in the cytoplasm to direct nascent ribosome−peptide complexes to the endoplasmic reticulum. SRP is functionally and structurally divided into two subunits, the "large" and "Alu" subunits (*5*−*8*). In mammalian cells, an SRP9/SRP14 heterodimer and approximately half of the RNA form the Alu subunit, which embodies the translational arrest activity of the SRP. The remaining four SRP proteins (SRP19, SRP54, SRP68, and SRP72) and the rest of the RNA comprise the large subunit (LS), which possesses the nascent peptide recognition and ER targeting activities of the SRP. Extensive studies have shown that the LS and Alu subunits of SRP assemble and function independently of each other (*7*−*9*). A closely related architecture is found in yeast (*10, 11*).

Although the SRP functions in the cytoplasm, studies with both mammalian (*12*−*14*) and yeast (*15, 16*) cells support a model (Figure 1B) in which all SRP proteins, except SRP54, are imported into the nucleolus/nucleus for assembly with the SRP RNA, whereupon the complex is exported back to the cytoplasm to bind SRP54. This model is also consonant with biochemical studies showing that SRP54 does not bind tightly to the free SRP RNA (*17, 18*). Instead, binding by SRP19 induces significant conformational changes in the SRP RNA and stabilizes an RNA conformation specifically recognized by SRP54 (*19*−*23*).

In this work we sought to determine whether physical segregation of SRP54 is a requirement for native assembly of the mammalian SRP. Using a three-component system composed of SRP RNA, SRP19, and SRP54, we used chemical probes to compare the structure of the complex formed by sequential addition of SRP19 and SRP54 to the RNA (the in vivo "SRP54-late" binding mechanism; Figure 1B,C) to that formed by the simultaneous presence of SRP19

† This work was supported by a grant from the National Institutes of Health (GM65491 to K.M.W.).

* Address correspondence to this author. E-mail: weeks@unc.edu.
‡ Department of Biochemistry and Biophysics.

10.1021/bi060890g CCC: $33.50
Published on Web 11/22/2006

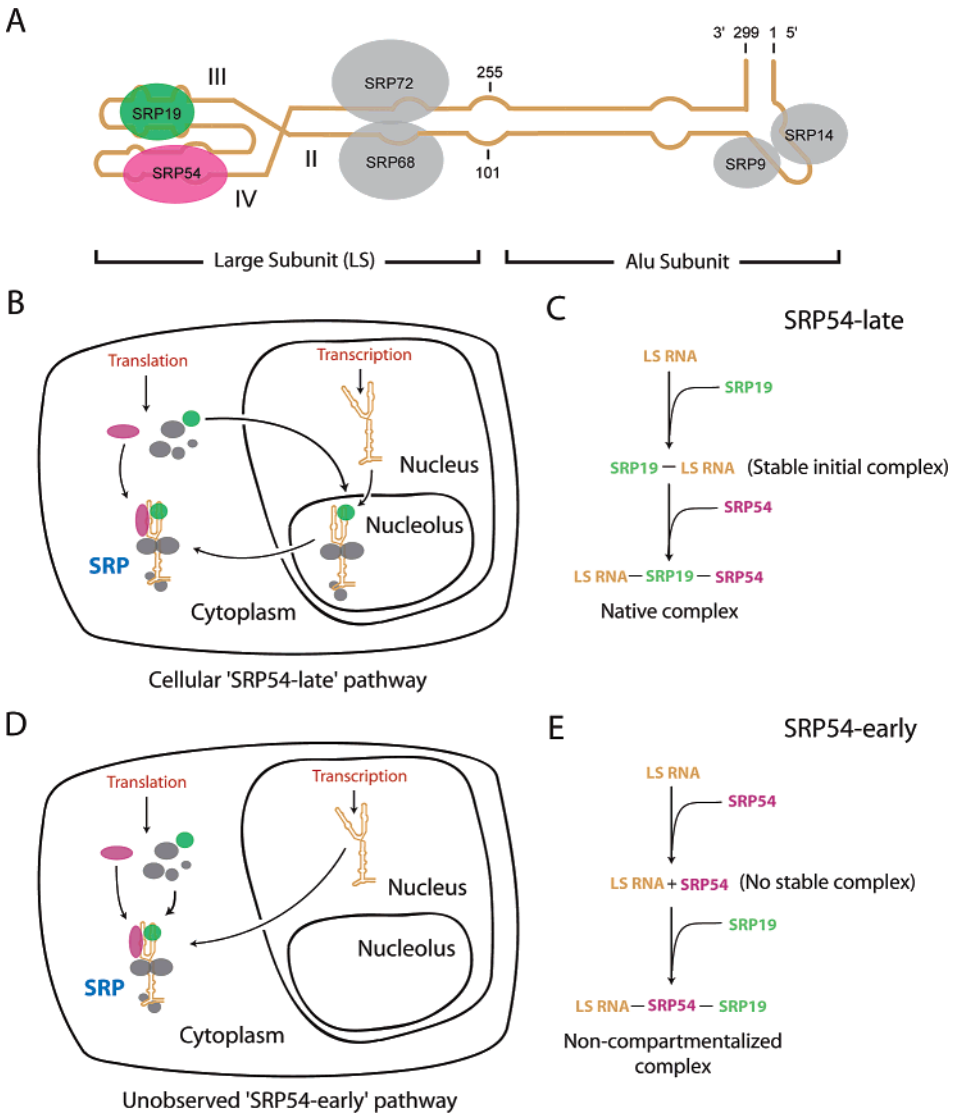

FIGURE 1: The signal recognition particle (SRP) and its compartmentalized cellular assembly. (A) Architecture of the mammalian SRP. SRP proteins are shown as colored or gray ovals; the RNA is in yellow. (B) Cellular SRP54-late pathway for SRP biogenesis (*12*, *13*, *15*, *16*, *30*). Five of six SRP proteins (SRP9, SRP14, SRP19, SRP68, and SRP72) enter the nucleolus and assemble with the SRP RNA. The partially assembled SRP is then transported back into the cytoplasm to bind SRP54 and form the native SRP holocomplex. (D) Unobserved simple pathway involving one-step SRP assembly in the cytoplasm. (C, E) Schemes for native SRP54-late versus unobserved SRP54-early assembly of SRP19, SRP54, and the LS RNA in vitro.

and SRP54 (the hypothetical "SRP54-early" pathway; Figure 1D,E). Notably, if SRP54 is present as SRP19 binds to the SRP RNA, we find that these three components interact to form a stable, alternate complex that is physically distinct from the native complex. These results strongly suggest that compartmentalizing SRP assembly into distinct cytoplasmic and nuclear phases is required to regulate native assembly of this ribonucleoprotein complex.

EXPERIMENTAL PROCEDURES

Proteins, RNA, Reaction Conditions, and Structure Visualization. Native SRP19 (*19*) and SRP54 (*24*) were expressed and purified as described, except that SRP54 was purified by Ni^{2+}−agarose and Bio-Rex columns. Final dialysis buffers contained 50% (v/v) glycerol. LS RNA (nts 101−255 of the human sequence) was transcribed from plasmid phR (*25*) and purified by denaturing electrophoresis. RNA was refolded by heating at 95 °C (1 min) and incubating at 60 °C (10 min) in the presence of RNA refolding buffer [300 mM potassium acetate (pH 7.6), 5 mM $MgCl_2$, 20 mM Hepes (pH 7.6), 0.01% (v/v) Triton], followed by slow cooling to room temperature (~40 min). All protein binding reactions were performed at 25 °C in RNA refolding buffer supplemented with $^1/_5$ volume of 300 mM NaCl, 50 mM sodium phosphate (pH 8.0), and 0.5 mg/mL BSA. SRP complexes were visualized using PyMOL (www.pymol.org).

Equilibrium Binding Measurements. 5′-^{32}P-end-labeled guanosine phosphorothioate-substituted LS RNA (0.3−0.5 nM) was incubated with SRP19, SRP54, or both at 25 °C in 20 μL. Bovine serum albumin (0.1 mg/mL; New England Biolabs) was present in the solution to prevent nonspecific protein binding. Complexes were incubated for 30 min, and cleavage was initiated by adding $^1/_{10}$ volume of 7 mM I_2. Reactions were quenched after 10 s by addition of $^1/_{10}$ volume of 70 mM 2-mercaptoethanol and an equal volume of formamide step dye. For measurements of SRP19-facilitated binding by SRP54, the SRP19 concentration was 15 nM and was added 15 min prior to addition of SRP54. Reaction

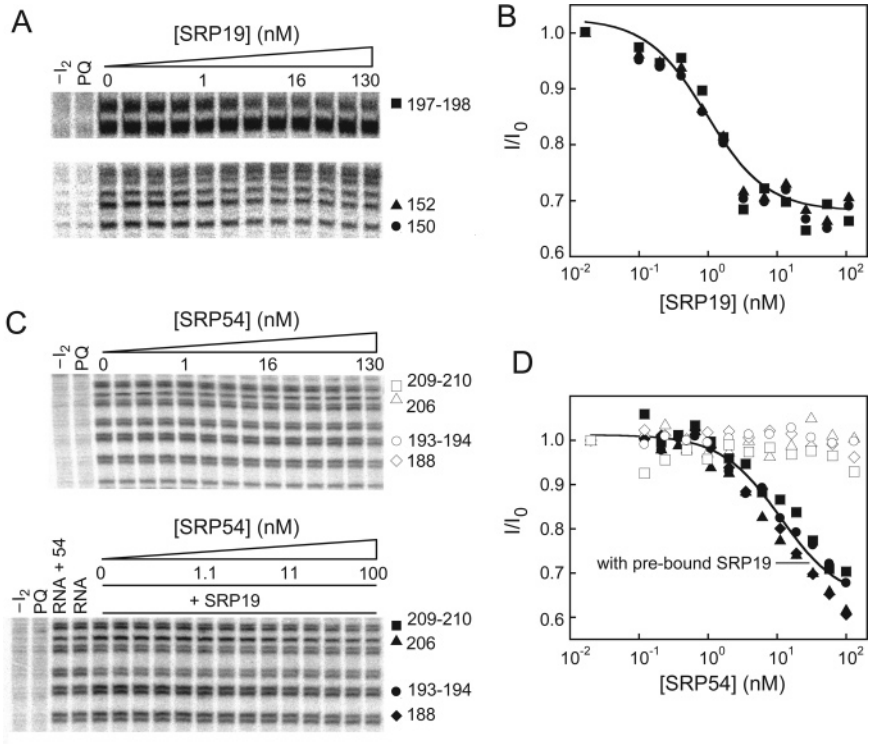

FIGURE 2: Equilibrium RNA binding by SRP19 and SRP54. (A) Affinity of the SRP19−LS RNA complex measured by phosphorothioate footprinting. Positions protected from iodine-mediated cleavage upon protein binding are indicated by solid symbols. Controls show experiments omitting iodine ($-I_2$) or in which the quench solution was added prior to iodine addition (prequench, PQ). (B) Quantitative analysis of SRP19 binding. I/I_0 is the observed band intensity normalized to the intensity observed in the absence of protein. Nucleotide symbols are the same as in (A). (C) High-affinity SRP54 binding requires prior binding by SRP19. Experiments performed in the absence (top panel) and presence (bottom panel) of SRP19 (15 nM) are indicated by open and closed symbols, respectively. (D) SRP54 binding to the free RNA (open symbols) or to a preformed SRP19−LS RNA complex (closed symbols).

products were resolved by denaturing electrophoresis, and band intensities (I) were quantified by phosphorimaging (Molecular Dynamics). Data were fit to $I/I_0 = K_d/(K_d + [\text{protein}]) + b$, where K_d is the equilibrium dissociation constant and b is the cleavage intensity at saturating protein concentration.

Phosphorothioate Footprinting Analysis of Native and Noncompartmentalized Complexes. All reactions (10 μL, 25 °C) contained identical buffer components and protein and RNA concentrations; final concentrations of SRP19, SRP54, and the LS RNA were 50, 100, and 10 nM, respectively. Assembly of the ternary complexes was performed by ordered addition of each protein to the RNA (SRP19 first or SRP54 first) followed by a 20 min incubation period. Iodine cleavage products were resolved in a series of 8−20% (w/v) denaturing gels. Lane integration was performed by phosphorimaging.

Expression, Purification, and Fe(II)-BABE Derivatization of SRP19 Variants. Four existing cysteines in the native sequence (C4S, C17V, C53V, and C94Y) were mutated to residues found in SRP19 proteins from other species using oligonucleotide-directed mutagenesis. This ΔCys parent construct was used to introduce unique cysteine residues at solvent-accessible positions (E31C, W72C, L93C, or L106C). SRP19 protein variants were expressed in *Escherichia coli* strain BL21-CodonPlus(DE3)-RIL (Stratagene) and purified as described (*19*). To conjugate SRP19 with Fe(II)-BABE (Pierce), 20 μL of each SRP19 variant protein (~20 μM) was treated with an equal volume of 8.5 mM Fe(II)-BABE [in 900 mM NaCl, 50 sodium phosphate (pH 8.0); 37 °C for 45 min]. Unreacted Fe(II)-BABE was removed by dialysis against 1 L of 900 mM NaCl, 50 mM sodium phosphate (pH 8.0), 10 mM 2-mercaptoethanol, and 25% (v/v) glycerol. As a control, the ΔCys parent protein was mock treated with Fe(II)-BABE in parallel with the single cysteine mutants. Equilibrium dissociation constants for all SRP19 proteins were measured by filter partitioning (*26*) using 0.1 nM internally labeled LS RNA. Dissociation constants were as follows [K_d, in nM; values for the Fe(II)-BABE derivatized protein are given in parentheses, errors are ±40% or less]: wild type, 2.0; ΔCys, 1.0; 31Cys, 15 (8); 72Cys, 6.0 (1.0); 93Cys, 10 (10); 106Cys, 10 (9.0). The dialyzed protein could be stored at −20 °C for at least 7 days without loss of RNA binding or cleavage activity.

Site-Directed Cleavage Experiments. Reactions (10 μL) contained 250 nM SRP19, SRP54, and refolded 5′-^{32}P-end-labeled LS RNA components, if present. Cleavage (3 min) was induced by addition of ascorbic acid and hydrogen peroxide to final concentrations of 10 mM and 0.3% (v/v), respectively, and quenched by addition of 10 μL of a 1:4 1 M thiourea:formamide solution containing 1% SDS. Cleaved RNA fragments were resolved in 10% denaturing polyacrylamide gels. Individual band intensities were integrated using SAFA (*27*), and site-specific cleavages were quantified by subtracting the background obtained for the ΔCys construct from cleavage intensity measured for the Fe(II)-BABE-conjugated SRP19 variants. For kinetic stability measurements, integrated band intensities were normalized at positions 148 and 198.

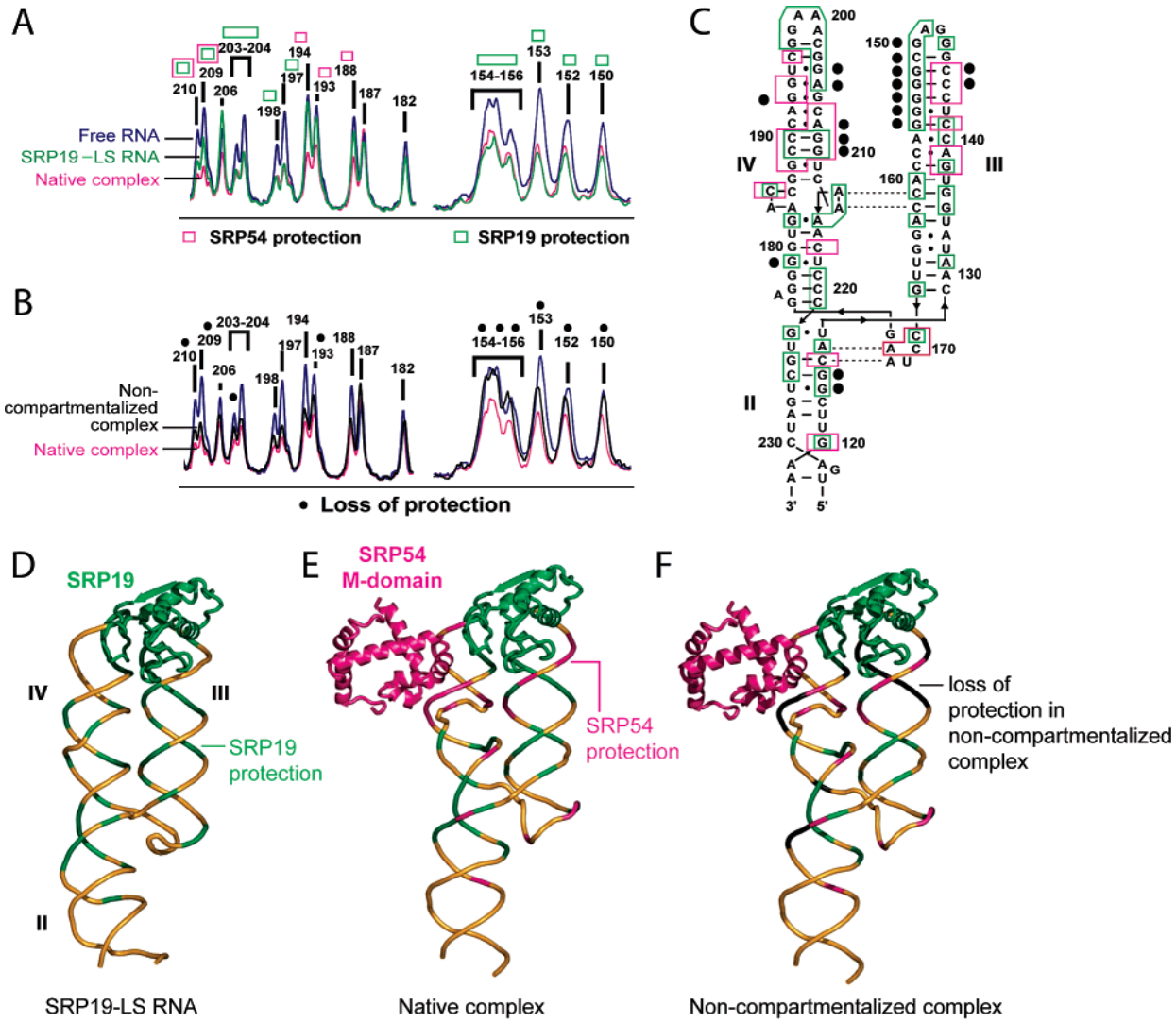

FIGURE 3: Distinct structures for SRP19−SRP54−LS RNA ternary complexes as a function of order of assembly. (A) Representative phosphorothioate footprinting cleavage intensities for the free LS RNA (blue), the SRP19−LS RNA complex (green), and the native SRP19−SRP54−LS RNA (purple) complex. Representative data for phosphorothioate-substituted guanosine residues are shown. Positions that become protected upon SRP19 or SRP54 binding are emphasized with green and purple boxes, respectively. (B) Phosphorothioate footprints illustrating structural differences in the ternary complexes assembled via SRP54-late (purple) versus SRP54-early (black) pathways. Sites where protection is reduced in the noncompartmentalized complex relative to the native complex are emphasized with black spheres. (C) Superposition of SRP19- and SRP54-induced protection (green and purple boxes, respectively) on the secondary structure of the LS RNA. Missing or reduced protections in the noncompartmentalized complex are indicated with black spheres. (D−F) SRP19- and SRP54-induced phosphorothioate footprints superimposed on three-dimensional structures for the SRP19−LS RNA binary (*21*) and the SRP19−SRP54−LS RNA ternary (*22*) complexes, respectively.

RESULTS

Cooperative RNA Binding by SRP19 and SRP54. We determined the affinities of SRP protein−RNA complexes by phosphorothioate footprinting (*19*, *28*). All experiments were performed with an RNA spanning the SRP large subunit (termed LS RNA, nts 101−255, Figure 1A). The LS RNA, SRP19, and SRP54 assemble independently of other SRP components (*7*, *9*, *22*). Equilibrium protein dissociation constants were monitored using an LS RNA carrying phosphorothioate substitutions at guanosine residues. For the free LS RNA, all phosphorothioate linkages were readily cleaved upon the addition of iodine (see 0 nM SRP19 lane, Figure 2A). Upon addition of SRP19, specific RNA positions became protected from cleavage (see G150, G152, and G197−198, Figure 2A). The equilibrium dissociation constant (K_d) for the SRP19−RNA complex was obtained by fitting the iodine-dependent cleavage intensity as a function of protein concentration to an equation for formation of a bimolecular complex. SRP19 binds the RNA with a K_d of 1.5 nM (Figure 2B), which agrees with previous values (2 nM) determined by conventional methods (*19*, *29*).

Similar phosphorothioate footprinting experiments were used to monitor binding of SRP54 to the free LS RNA (upper panel, Figure 2C). SRP54 binding was undetectable at protein concentrations up to 500 nM (open symbols, Figures 2C,D). In contrast, when SRP54 bound to a preformed SRP19−RNA complex, specific phosphorothioate-substituted guanosine nucleotides became additionally protected from cleavage (lower panel, Figure 2C). SRP54 bound to the preorganized SRP19−RNA complex with an equilibrium K_d of 12 nM (solid symbols, Figure 2D).

In summary, SRP54 does not form a stable complex with the SRP RNA at a concentration as high as 500 nM while prior binding by SRP19 enhances SRP54 binding affinity by at least 40-fold.

Strategy for Evaluating the Role of Compartmentalization in SRP Assembly. In the cell, SRP54 appears to interact with the SRP RNA in the cytoplasm and only after the RNA has formed a complex with SRP19 (*12*, *13*, *15*, *16*, *30*): we term this the SRP54-late assembly model. In this work, we used order-of-addition experiments to evaluate whether allowing SRP19 and SRP54 to assemble simultaneously with the SRP RNA affects the structure of the final SRP19−SRP54−RNA ternary complex.

In our in vitro scheme for assembling a native ternary complex, we followed the SRP54-late pathway by first allowing a stable SRP19−RNA complex to form and then adding SRP54 (illustrated in Figure 1C). To model the hypothetical situation in which SRP19, SRP54, and the SRP RNA are free to assemble in the same compartment and during the same time interval, we performed in vitro experiments in which we simply added SRP19 to a mixture of free LS RNA and free SRP54 (Figure 1E). Recall that SRP54 does not form a stable complex with the free LS RNA (Figure 2D). Thus, formation of any complex containing SRP54 must be induced by a binding event involving SRP19. We term this pathway SRP54-early assembly, and the ternary complex formed via this pathway is called the "noncompartmentalized" complex.

Structure of the Native SRP19−SRP54−RNA Ternary Complex. In an approach similar to that used to measure protein dissociation constants above, we also used phosphorothioate footprinting to quantify the accessibility of every nucleotide in SRP complexes. Protection from iodine-mediated cleavage reflects both direct occlusion of the RNA backbone and protein-induced conformational changes in the RNA (*19*, *31*, *32*). Importantly, because changes in individual band intensities can be normalized to the many nucleotides whose reactivity does not change, even small changes in local environment are robustly scored by the phosphorothioate footprinting approach (*32*).

Cleavage intensities were quantified for entire sequencing gel lanes and representative data for experiments performed with RNAs containing phosphorothioate-substituted guanosine residues are shown in Figure 3A,B. In both panels, blue traces indicate cleavage intensities observed for the free LS RNA.

When phosphorothioate footprinting was performed on the SRP19−RNA complex, many nucleotides became protected from cleavage, as expected (SRP19 protection is summarized as green boxes in Figure 3A). Data obtained by evaluating LS RNAs containing each of the four phosphorothioate-substituted nucleotides are summarized in Figure 3C and are superimposed as a green backbone on a crystallographic structure for this complex (Figure 3D). SRP19-induced protection from iodine-mediated cleavage occurs exactly at the protein−RNA interface, in RNA regions that lie in close contact in the binary complex, and in structures that undergo a conformational change upon protein binding (Figure 3D).

We then evaluated structural changes that occur when SRP54 binds to a preformed SRP19−RNA complex (purple trace in Figure 3A). Nucleotides showing specific protection upon addition of SRP54 are emphasized with purple boxes and are summarized in the context of a secondary structure for the LS RNA in Figure 3C. Positions that show new or enhanced protection from iodine-mediated cleavage are largely localized at the SRP54 binding site and at neighboring regions in helix III, as visualized in the context of the three-dimensional structure for this ternary complex (Figure 3E). The excellent correlation between the footprinting experiments and the three-dimensional structures for these complexes (Figure 3D,E) indicates that phosphorothioate footprinting accurately reports protein binding sites and protein-induced conformational changes in the SRP RNA.

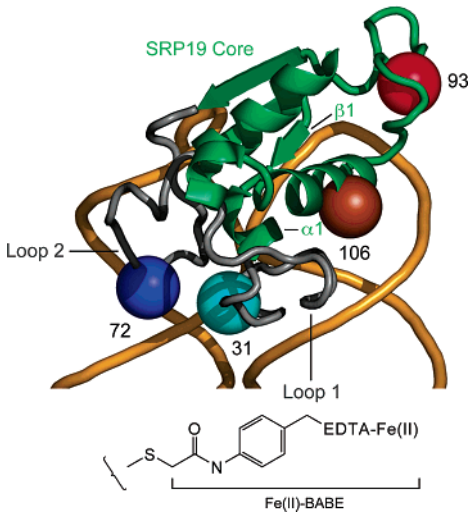

FIGURE 4: SRP19 structure and sites of Fe(II)-BABE derivatization. The SRP19 core is in green, and RNA-binding loops are in gray. Sites of unique cysteine residues used for site-specific conjugation with the Fe(II)-BABE reagent are shown as spheres.

SRP Ternary Complexes Formed via the SRP54-Late versus SRP54-Early Pathways Are Distinct. Next, we evaluated the structural consequences if the SRP19−SRP54−RNA complex assembles via the SRP54-early pathway (Figure 1E). Importantly, the final solution compositions were the same for complexes formed via either pathway but differed only in the order of addition of SRP19 and SRP54.

For many positions, the observed protection was identical for complexes formed via either pathway (for example, see positions 187−188 and 197−198 in Figure 3A,B). In strong contrast, at many other positions, protection from iodine-mediated cleavage was significantly reduced for complexes formed by adding SRP54 prior to SRP19 (emphasized with filled spheres in Figure 3B,C). Superposition of these weaker and missing protections on the three-dimensional structure of the SRP19−SRP54−RNA ternary complex indicates that structural changes occur in RNA regions close to both SRP19 and SRP54 binding sites (black backbone, Figure 3F).

These phosphorothioate footprinting experiments thus demonstrate that structurally distinct complexes form depending on whether SRP54 is present or absent as SRP19 assembles with the RNA.

SRP19−RNA Interactions Mapped by Site-Directed Cleavage. The phosphorothioate footprinting experiments provide definitive evidence that the structures of SRP complexes formed via the SRP54-late and SRP54-early pathways are different. We then used site-directed hydroxyl radical cleavage to obtain detailed views of the structural differences in these two ternary complexes.

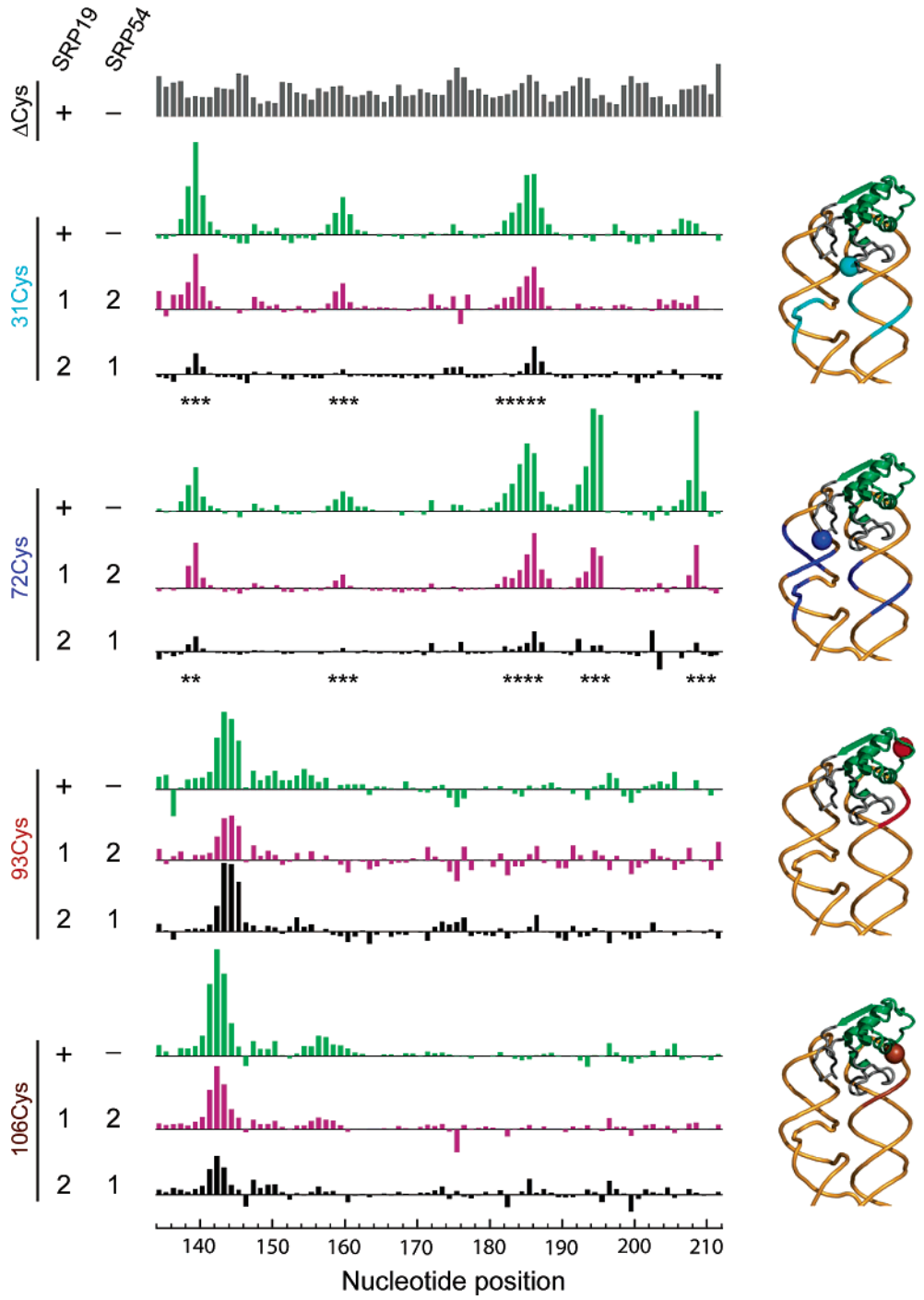

FIGURE 5: SRP19 structure in the native and noncompartmentalized ternary complexes analyzed by site-directed hydroxyl radical cleavage. RNA cleavage intensity histograms are shown for each SRP19 variant, after subtracting cleavage intensity for the ΔCys parent construct. Key: green, binary SRP19−LS RNA complexes; purple, native ternary complexes (SRP54-late pathway); black, noncompartmentalized ternary complexes (SRP54-early pathway). Site-specific cleavages that are absent or severely reduced in the noncompartmentalized complex are emphasized with asterisks. Right-hand panels show site-directed cleavage information for the binary SRP19−RNA complexes superimposed on its three-dimensional structure.

In a complex with the SRP RNA, the SRP19 protein spans two structural elements (*22*). SRP19 contains a core domain comprised of a three-stranded β-sheet packed against two α-helices. The second structural element is comprised of two irregular loops that extend from the SRP19 core (Figure 4). Direct contacts with the SRP RNA involve multiple interactions mediated by the two irregular loops, plus contacts mediated by residues extending from the first β-strand and the first α-helix in the core (β1 and α1 in Figure 4, respectively). We therefore monitored interactions between the RNA and SRP19 by performing site-directed cleavage experiments using the Fe(II)-BABE reagent tethered at both SRP19 core and loop regions (Figure 4).

Four cysteine residues in the native SRP19 sequence were mutated to create a ΔCys parent construct. Unique solvent-accessible cysteine residues were then individually introduced into each of the two RNA-binding loops (at positions 31 and 72) and into the SRP19 core (at positions 93 and 106) (colored spheres in Figure 4). RNA-binding affinities for each SRP19 variant were within 3−8 fold of that for the wild-

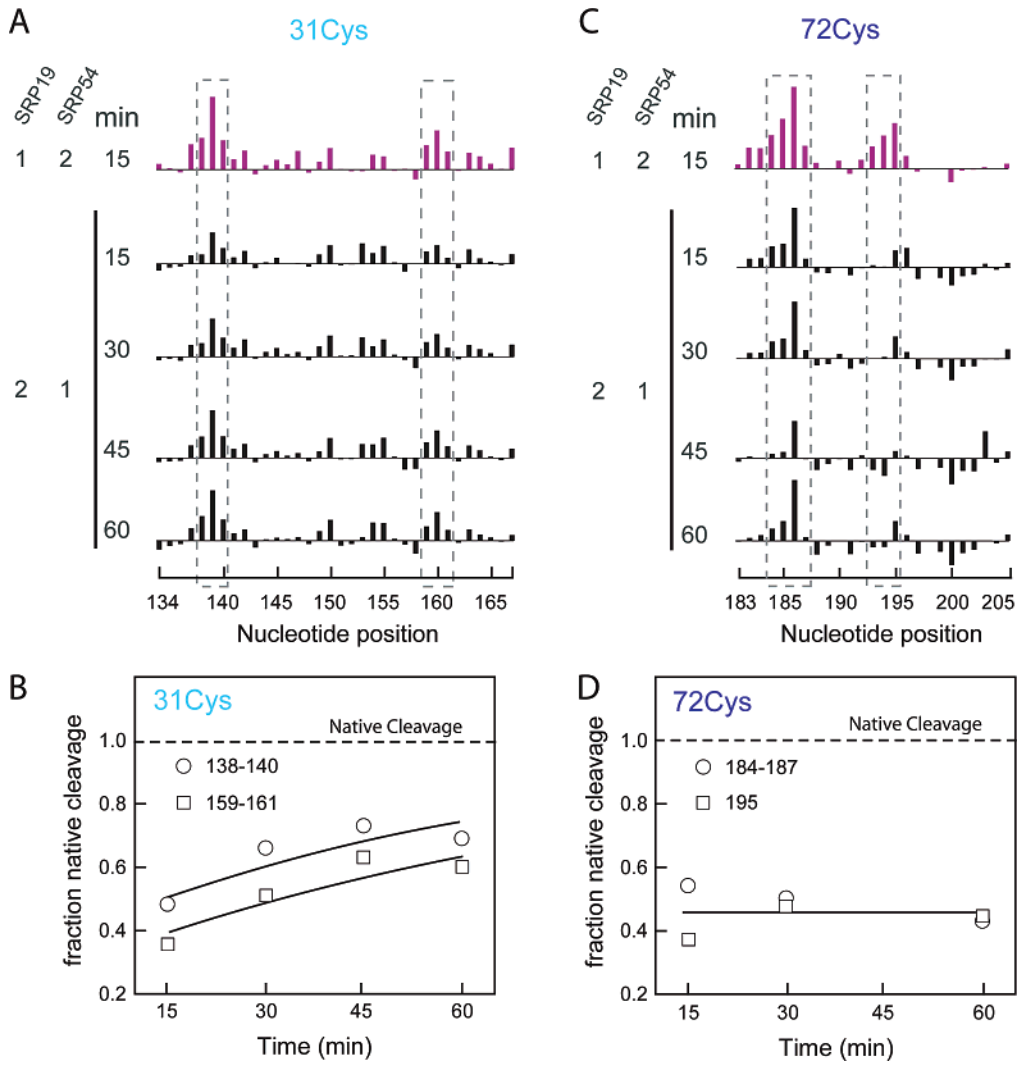

FIGURE 6: Kinetic stability of the noncompartmentalized complex. (A, C) Site-directed hydroxyl radical cleavage. SRP19 and SRP54 were added in the orders shown. Site-directed cleavage from position 31 or 72 was initiated at varying times after initial complex formation. RNA sites where cleavage is selectively lost in the noncompartmentalized ternary complex are emphasized with dashed boxes. (B, D) Recovery of native cleavage patterns as a function of time. Data for 31Cys were fit to a single exponential, whereas no detectable recovery was observed for the 72Cys protein after 1 h.

type protein. Conjugation with Fe(II)-BABE had no additional effect on binding for any of the SRP19 variants.

Site-directed cleavage experiments were initially performed for simple binary complexes containing the LS RNA and each of the four SRP19 proteins. Upon addition of reagents, the tethered Fe(II)-BABE group produced hydroxyl radicals that cleaved nearby regions of the RNA backbone. Specific cleavages were identified relative to mock reactions performed using the ΔCys parent construct (Figure 5, green histograms). SRP19 variants derivatized at either of the two RNA-binding loops (positions 31 and 72) and at the core (positions 93 and 106) yield distinctive and nonoverlapping cleavage patterns at the SRP RNA backbone that are exactly consistent with the structure of this complex (see structures on the right-hand side of Figure 5). Thus, site-directed cleavage experiments accurately report native RNA−protein interactions mediated by both the RNA-binding loops and core domain of SRP19.

RNA-Binding Loops Fold Differently in the Noncompartmentalized Complex. We evaluated the structural consequences of forming the SRP19−SRP54−LS RNA ternary complex by each of the two assembly pathways. When site-directed hydroxyl radical cleavage experiments were performed on the native ternary complex (formed via the SRP54-late pathway), the pattern of cleavage was largely unchanged for all four SRP19 constructs (compare green and purple histograms, Figure 5).

When identical hydroxyl cleavage experiments were performed on the noncompartmentalized complex (formed via the SRP54-early pathway), cleavage intensities using SRP19 derivatized in the core (positions 93 and 106) were essentially identical to those observed for the native complex (see black histograms for 93Cys and 106Cys SRP19 variants; lower panels, Figure 5). In strong contrast, when the structure of the noncompartmentalized complex was monitored using SRP19 proteins derivatized with Fe(II)-BABE at loop 1 or loop 2, specific RNA cleavages were either missing or significantly reduced in intensity (see black histograms for 31Cys and 72Cys, respectively; upper panels, Figure 5). These results indicate that the SRP19 core domain interacts similarly with the LS RNA in both native and noncompartmentalized complexes while SRP19 loops 1 and 2 fail to form native interactions with the RNA when the ternary complex is formed via the SRP54-early pathway.

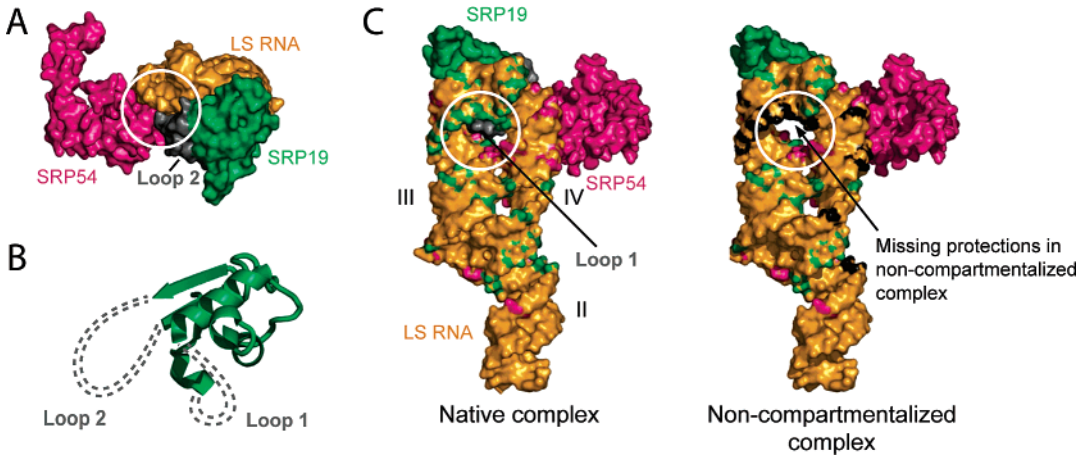

FIGURE 7: Structures for native and noncompartmentalized SRP complexes. (A) Intimate contacts among SRP19, SRP54, and LS RNA in the native ternary complex. Loop 2 in SRP19 (in gray) is sandwiched between SRP54 and the RNA (white circle). (B) Schematic structure for SRP19 in the noncompartmentalized complex. (C) RNA sites that interact with SRP19 loop 1 in the native complex coincide with positions at which protection from iodine-mediated cleavage is lost in the noncompartmentalized complex (black surface).

The Noncompartmentalized Complex Is Stable. We evaluated the kinetic stability of the noncompartmentalized complex by monitoring recovery of the 31Cys and 72Cys cleavages as a function of time. We compared site-directed cleavage intensities observed for the complex formed via the SRP54-early pathway to those observed in the native complex. For the 31Cys protein, cleavage intensities at positions 138−140 and 159−161 recover slowly over a period of 1 h (Figure 6A). The rate constant for achieving a native-like cleavage pattern is 0.013 min^{-1}, corresponding to a half-life of 54 min (Figure 6B). In contrast, the cleavage pattern of the 72Cys protein shows no detectable recovery to the native conformation over 1 h (Figure 6C,D). These results demonstrate that the noncompartmentalized complex is extremely stable and that the two RNA-binding loops rearrange to a native-like conformation at different rates: recovery of loop 2 is much slower than loop 1.

DISCUSSION

Protein-Mediated Disruption of Native RNP Assembly. To date, essentially all models for assembly of multicomponent ribonucleoproteins, including the ribosome, tacitly assume that binding by any given protein component either facilitates further RNP assembly or has no effect on continued assembly. Our experiments reveal an unanticipated and additional dimension to RNP biogenesis, namely, that an untimely interaction can disrupt formation of the native RNP. We show that SRP54 is able to interfere with native assembly of SRP19 with the SRP RNA in vitro, a situation which is presumably avoided in vivo by differential nuclear and cytoplasmic compartmentalization.

Structure of the Noncompartmentalized Complex. Together with crystallographic structures for the SRP19−RNA binary (*21*) and SRP19−SRP54−RNA ternary (*22*) complexes, our nucleotide resolution solution-phase experiments allow us to develop a structural model for the (noncompartmentalized) ternary complex formed via the SRP54-early pathway. In the native ternary complex, SRP19, SRP54, and the SRP RNA each contact both of the other two components (circled, Figure 7A). Contacts between SRP19 and the RNA in the native complex are mediated by two loops that extend from the core of the protein plus additional interactions involving the first β-strand and first α-helix in the core (Figure 4). SRP19 is a natively unfolded protein, and these RNA-binding loops, especially, are only likely to fold to their native conformations when bound to RNA.

When the Fe(II)-BABE reagent was attached at position 93 or 106 in the SRP19 core, hydroxyl radical RNA cleavages were similar in both native and noncompartmentalized complexes. In strong contrast, when the cleavage agent was attached at the RNA-binding loops (positions 31 and 72), RNA cleavages were either greatly reduced or missing altogether in the noncompartmentalized complex. We infer that, in the noncompartmentalized complex, the SRP19 core is positioned on the RNA in a manner similar to that in the native complex, whereas loops 1 and 2 misfold and fail to form native contacts with the RNA (Figure 7B). This structural interpretation is supported by iodine-mediated phosphorothioate footprinting experiments. In the native complex, loop 1 fills a hole in the RNA fold and results in phosphorothioate footprinting protection on the RNA face opposite to where SRP19 binds (see circle in Figure 7C). In the noncompartmentalized complex, loop 1 misfolds, and backbone groups at the circumference of the internal hole in the RNA show enhanced reactivities relative to the native complex (black surface residues, Figure 7C). Residues that interact with loop 2 also show enhanced phosphorothioate reactivities in the noncompartmentalized complex at positions 204 and 205 in helix IV of the RNA (see Figure 3F).

Mechanisms for SRP54-Late and SRP54-Early Assembly. Two additional pieces of information allow us to propose mechanisms for SRP54-late versus SRP54-early assembly of the SRP19−SRP54−RNA ternary complex. First, inspection of the protein−RNA interfaces in the native ternary complex (Figure 7A) suggests that SRP54 abuts the other two components and can, in principle, bind approximately as a rigid unit to a partially formed SRP19−RNA complex. In contrast, binding by SRP19 requires that loop 2 be inserted *under* the existing SRP54−RNA interface. If this "folding under" step were sterically disfavored, a non-native complex would result in which loop 2 in SRP19 is misfolded. Loop 1 would also presumably misfold because folding of loop 1 and loop 2 appears to be linked.

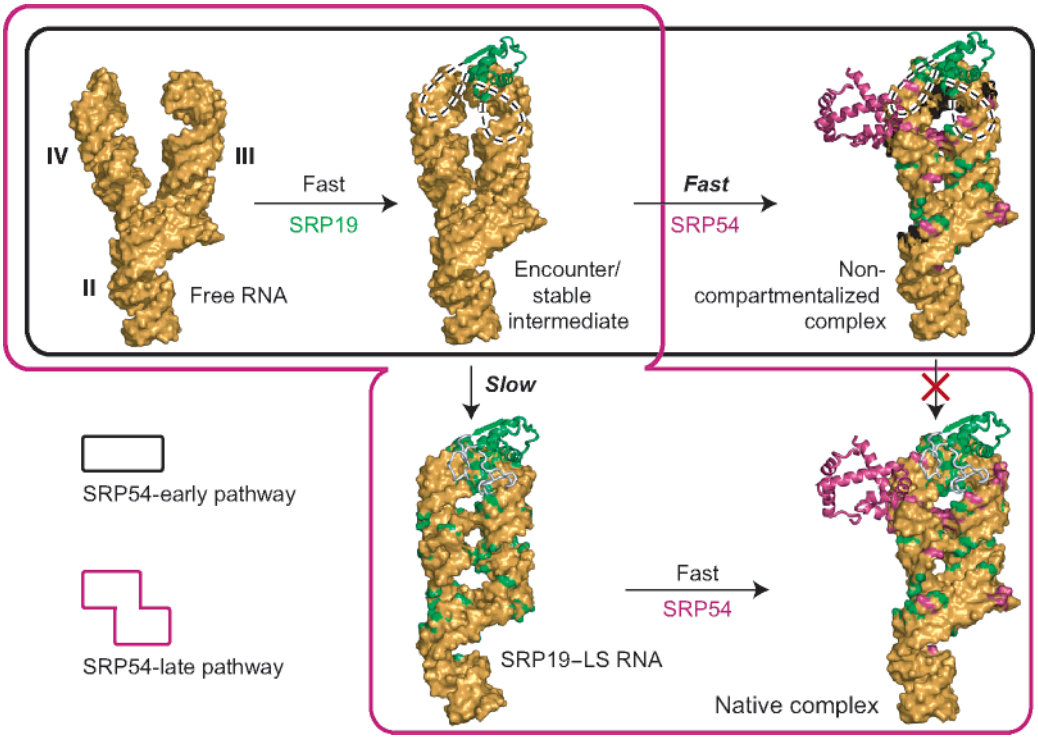

FIGURE 8: Assembly of the SRP19−SRP54−LS RNA ternary complex via an intermediate state involving partially folded SRP19. SRP54-late and SRP54-early pathways are emphasized in purple and black boxes, respectively. The RNA surface is in yellow; positions protected by SRP19 or SRP54 are in green and purple, respectively. Missing protections in the noncompartmentalized complex are in black. The red × indicates that the noncompartmentalized complex converts to the native complex very slowly.

Second, binding by SRP19 to the RNA involves formation of at least two intermediate complexes, termed the encounter and stable complexes, that form with fast kinetics (*19*). Subsequently, the intermediate complexes fold slowly to form the native complex:

$$\text{RNA} + \text{SRP19} \xrightarrow{\text{fast}} \text{encounter/stable} \xrightarrow{\text{slow}} \text{SRP19}-\text{RNA}$$

In our proposed mechanism for assembly of the SRP19−SRP54−RNA ternary complex, the free RNA is initially in a relatively open conformation as supported by the absence of a stable hydroxyl radical footprint (see free RNA, Figure 8) (*19*). SRP19 binds rapidly to the free RNA to form the encounter/stable intermediate. In the intermediate complex, the SRP19 core interacts in a near-native way with the RNA, whereas loops 1 and 2 do not form native interactions with the RNA (see intermediate complex, Figure 8). In the intermediate complex, sufficient global reorganization of the RNA has occurred to permit stable binding by SRP54. Formation of this intermediate complex is the same for assembly via either SRP54-late or SRP54-early pathways.

If SRP54 is not present at this stage, previous work (*19*) shows that the SRP19−RNA complex resolves slowly to a native bimolecular complex (lower pathway, Figure 8). Once the stage requiring compartmentalized assembly is completed, SRP54 can bind to the SRP19−RNA complex to form the native ternary complex. Native ternary complex formation involves additional conformational changes in the RNA (purple regions in the native complex, Figure 8).

In contrast, if SRP54 is present during the phase when the encounter/stable intermediate forms, SRP54 binds rapidly to the preorganized RNA to form the noncompartmentalized complex. The noncompartmentalized complex is characterized by some of the same SRP54-induced changes that occur in the native ternary complex. However, early binding by SRP54 inhibits some SRP19 folding events that take place during slow conversion of the intermediate SRP19−RNA complex into the native SRP19−RNA complex. As a result, RNA-binding loops 1 and 2 remain misfolded in the noncompartmentalized complex (see dashed protein loops and black RNA backbone in noncompartmentalized complex, Figure 8).

Role of Compartmentalization To Sequester Immature RNPs during Assembly. Our results show that SRP54 can disrupt native SRP19−RNA assembly, implying that SRP54 must be sequestered, as apparently occurs in vivo, for proper assembly of the SRP to occur. Given the profound effect of compartmentalization on assembly of this relatively simple three-component system, cellular compartmentalization may broadly direct native assembly of other multicomponent RNPs.

REFERENCES

1. Pederson, T., and Politz, J. C. (2000) The nucleolus and the four ribonucleoproteins of translation, *J. Cell Biol. 148*, 1091−1095.
2. Filipowicz, W., and Pogacic, V. (2002) Biogenesis of small nucleolar ribonucleoproteins, *Curr. Opin. Cell Biol. 14*, 319−327.
3. Gerbi, S. A., Borovjagin, A. V., and Lange, T. S. (2003) The nucleolus: a site of ribonucleoprotein maturation, *Curr. Opin. Cell Biol. 15*, 318−325.
4. Fromont-Racine, M., Senger, B., and Saveanu C. F. F. (2003) Ribosome assembly in eukaryotes, *Gene 313*, 17−42.
5. Keenan, R. J., Freymann, D. M., Stroud, R. M., and Walter, P. (2001) The signal recognition particle, *Annu. Rev. Biochem. 70*, 755−775.
6. Nagai, K., Oubridge, C., Kuglstatter, A., Menichelli, E., Isel, C., and Jovine, L. (2003) Structure, function and evolution of the signal recognition particle, *EMBO J. 22*, 3479−3485.

7. Halic, M., Becker, T., Pool, M. R., Spahn, C. M. T., Grassucci, R. A., Frank, J., and Beckmann, R. (2004) Structure of the signal recognition particle interacting with the elongation-arrested ribosome, *Nature 427*, 808−814.
8. Egea, P. F., Stroud, R. M., and Walter, P. (2005) Targeting proteins to membranes: structure of the signal recognition particle, *Curr. Opin. Struct. Biol. 15*, 213−220.
9. Siegel, V., and Walter, P. (1988) Each of the activities of signal recognition particle (SRP) is contained within a distinct domain: Analysis of biochemical mutants of SRP, *Cell 52*, 39−49.
10. Hann, B. C., and Walter, P. (1991) The signal recognition particle in *S. cerevisiae*, *Cell 67*, 131−144.
11. Brown, J. D., Hann, B. C., Medzihradszky, K. F., Niwa, M., Burlingame, A. L., and Walter, P. (1994) Subunits of the *Saccharomyces cerevisiae* signal recognition particle required for its functional expression, *EMBO J. 13*, 4390−4000.
12. Jacobson, M. R., and Pederson, T. (1998) Localization of signal recognition particle RNA in the nucleolus of mammalian cells, *Proc. Natl. Acad. Sci. U.S.A. 95*, 7981−7986.
13. Politz, J. C., Yarovoi, S., Kilroy, S. M., Gowda, K., Zwieb, C., and Pederson, T. (2000) Signal recognition particle components in the nucleolus, *Proc. Natl. Acad. Sci. U.S.A. 97*, 55−60.
14. Alavian, C. N., Politz, J. C. R., Lewandowski, L. B., Powers, C. M., and Pederson, T. (2004) Nuclear export of signal recognition particle RNA in mammalian cells, *Biochem. Biophys. Res. Commun. 313*, 351−355.
15. Ciufo, L. F., and Brown, J. D. (2000) Nuclear export of yeast signal recognition particle lacking Srp54p by the Xpo1p/Crm1p NES-dependent pathway, *Curr. Biol. 10*, 1256−1264.
16. Grosshans, H., Deinert, K., Hurt, E., and Simos, G. (2001) Biogenesis of the signal recognition particle (SRP) involves import of SRP proteins into the nucleolus, assembly with the SRP-RNA, and Xpo1p-mediated export, *J. Cell Biol. 153*, 745−761.
17. Gowda, K., Chittenden, K., and Zwieb, C. (1997) Binding site of the M-domain of human protein SRP54 determined by systematic site-directed mutagenesis of signal recognition particle RNA, *Nucleic Acids Res. 25*, 388−394.
18. Romisch, K., Webb, J., Herz, J., Prehn, S., Frank, R., Vingron, M., and Dobberstein, B. (1989) Homology of 54K protein of signal-recognition particle, docking protein and two *E. coli* proteins with putative GTP-binding domains, *Nature 340*, 478−482.
19. Rose, M. A., and Weeks, K. M. (2001) Visualizing induced fit in early assembly of the human signal recognition particle, *Nat. Struct. Biol. 8*, 515−520.
20. Diener, J. L., and Wilson, C. (2000) Role of SRP19 in assembly of the *Archaeoglobus fulgidus* signal recognition particle, *Biochemistry 39*, 12862−12874.
21. Oubridge, C., Kuglstatter, A., Jovine, L., and Nagai, K. (2002) Crystal structure of SRP19 in complex with the S domain of SRP RNA and its implication for the assembly of the signal recognition particle, *Mol. Cell 9*, 1251−1261.
22. Kuglstatter, A., Oubridge, C., and Nagai, K. (2002) Induced structural changes of 7SL RNA during the assembly of human signal recognition particle, *Nat. Struct. Biol. 9*, 740−744.
23. Hainzl, T., Huang, S., and Sauer-Eriksson, A. E. (2005) Structural insights into SRP RNA: an induced fit mechanism for SRP assembly, *RNA 11*, 1043−1050.
24. Gowda, K., Black, S. D., Moeller, I., Sakakibara, Y., Liu, M.-C., and Zwieb, C. (1998) Protein SRP54 of human signal recognition particle: Cloning, expression, and comparative analysis of functional sites, *Gene 207*, 197−207.
25. Zwieb, C. (1991) Interaction of protein SRP19 with signal recognition particle RNA lacking individual RNA-helices, *Nucleic Acids Res. 19*, 2955−2960.
26. Weeks, K. M., and Cech, T. R. (1995) Efficient protein-facilitated splicing of the yeast mitochondrial bI5 intron, *Biochemistry 34*, 7728−7738.
27. Das, R., Laederach, A., Pearlman, S. M., Herschlag, D., and Altman, R. B. (2005) Semi-automated footprinting analysis software for high-throughput quantification of nucleic acid footprinting experiments, *RNA 11*, 344−354.
28. Schatz, D., Leberman, R., and Eckstein, F. (1991) Interaction of *Escherichia coli* $rRNA^{Ser}$ with its cognate aminoacyl-rRNA synthetase as determined by footprinting with phosphorothioate-containing rRNA transcripts, *Proc. Natl. Acad. Sci. U.S.A. 88*, 6132−6136.
29. Henry, K. A., Zwieb, C., and Fried, H. M. (1997) Purification and biochemical characterization of the 19-kDa signal recognition particle RNA-binding protein expressed as a hexahistidine-tagged polypeptide in *Escherichia coli*, *Protein Expression Purif. 9*, 15026−15033.
30. Dean, K. A., von Ahsen, O., Gorlich, D., and Fried, H. M. (2001) Signal recognition particle protein 19 is imported into nucleus by importin 8 (RanBP8) and transportin, *J. Cell Sci. 114*, 3479−3485.
31. Webb, A. E., Rose, M. A., Westhof, E., and Weeks, K. M. (2001) Protein-dependent transition states for ribonucleoprotein assembly, *J. Mol. Biol. 309*, 1087−1100.
32. Garcia, I., and Weeks, K. M. (2004) Structural basis for the self-chaperoning function of an RNA collapsed state, *Biochemistry 43*, 15179−15186.

BI060890G